Knockdown of *ttc26* disrupts ciliogenesis of the photoreceptor cells and the pronephros in zebrafish

Qi Zhang[a], Qin Liu[a], Chrissy Austin[b], Iain Drummond[b], and Eric A. Pierce[a]
[a]Ocular Genomics Institute & Berman-Gund Laboratory, Department of Ophthalmology, Massachusetts Eye and Ear Infirmary, Harvard Medical School, Boston, MA 02114; [b]Renal Unit-CNY 8, Massachusetts General Hospital, Harvard Medical School, Charlestown, MA 02129

ABSTRACT **In our effort to understand genetic disorders of the photoreceptor cells of the retina, we have focused on intraflagellar transport in photoreceptor sensory cilia. From previous mouse proteomic data we identified a cilia protein Ttc26, orthologue of dyf-13 in *Caenorhabditis elegans*, as a target. We localized Ttc26 to the transition zone of photoreceptor and to the transition zone of cilia in cultured murine inner medullary collecting duct 3 (mIMCD3) renal cells. Knockdown of *Ttc26* in mIMCD3 cells produced shortened and defective primary cilia, as revealed by immunofluorescence and scanning electron microscopy. To study Ttc26 function in sensory cilia in vivo, we utilized a zebrafish vertebrate model system. Morpholino knockdown of *ttc26* in zebrafish embryos caused ciliary defects in the pronephric kidney at 27 h postfertilization and distension/dilation of pronephros at 5 d postfertilization (dpf). In the eyes, the outer segments of photoreceptor cells appeared shortened or absent, whereas cellular lamination appeared normal in retinas at 5 dpf. This suggests that loss of ttc26 function prevents normal ciliogenesis and differentiation in the photoreceptor cells, and that ttc26 is required for normal development and differentiation in retina and pronephros. Our studies support the importance of Ttc26 function in ciliogenesis and suggest that screening for *TTC26* mutations in human ciliopathies is justified.**

Monitoring Editor
Erika Holzbaur
University of Pennsylvania

Received: Jan 10, 2012
Revised: Jun 7, 2012
Accepted: Jun 12, 2012

INTRODUCTION

Inherited retinal degenerations (IRDs) are important causes of blindness (Pierce, 2001). These disorders are characterized by dysfunction and death of photoreceptor cells of the retina. The light-sensitive outer segments of photoreceptor cells are specialized sensory cilia, and the importance of primary and sensory cilia in biology and disease is becoming increasingly recognized (Singla and Reiter, 2006; Breunig *et al.*, 2008; Simons and Mlodzik, 2008; Slough *et al.*, 2008). Primary cilia are present on most vertebrate cell types, and these structures are typically sensory organelles involved in many critical aspects of cell biology, such as signal transduction pathways and generating and detecting fluid flow (Pazour and Witman, 2003; Pan *et al.*, 2005).

The rod and cone photoreceptors are among the largest of mammalian cilia (Pan *et al.*, 2005; Yang *et al.*, 2005). Like other cilia, the outer segments contain an axoneme, which begins at the basal bodies and passes through a transition zone (also called the "connecting cilium") and into the outer segments (Beisson and Wright, 2003). The photoreceptor sensory cilium (PSC) comprises the outer segment and its cytoskeleton, including the rootlet, basal body, and axoneme (Liu *et al.*, 2007). The membrane of outer segments is highly specialized for light detection, with the proteins required for

This article was published online ahead of print in MBoC in Press (http://www.molbiolcell.org/cgi/doi/10.1091/mbc.E12-01-0019) on June 20, 2012.

Address correspondence to: Eric Pierce (eric_pierce@meei.harvard.edu).

Abbreviations used: BBS, Bardet-Biedl syndrome; bps, beats per second; BSA, bovine serum albumin; dpf, days postfertilization; EGFP, enhanced green fluorescent protein; FBS, fetal bovine serum; GFP, green fluorescent protein; hpf, hours postfertilization; IFT, intraflagellar transport; IgG, immunoglobulin G; IRD, inherited retinal degenerations; LCA, Leber congenital amaurosis; mAb, monoclonal antibody; mIMCD3, murine inner medullary collecting duct 3 cells; MO, morpholino oligonucleotides; MZ, marginal zones; PBS, phosphate-buffered saline; PSC, photoreceptor sensory cilium; RNAi, RNA interference; RP, retinitis pigmentosa; RT-PCR, reverse transcriptase PCR; SEM, scanning electron microscopy; shRNA, short hairpin RNA; SSTR3, somatostatin receptor 3; TEM, transmission electron microscopy; TPR, tetratricopeptide repeats.

phototransduction located in or associated with the membrane disks stacked in tight order at ~30 per micron along the axoneme. The transition zone in PCS is analogous to transition zones in other cilia and is where the triplet microtubule structure of the basal bodies converts to the doublet microtubule structure of the axoneme (Horst *et al.*, 1990).

The recognition of photoreceptor outer segments as cilia connects retinal degenerative disorders such as retinitis pigmentosa (RP) and Leber congenital amaurosis (LCA) to other ciliary disorders. Mutations in genes that encode cilia proteins are increasingly recognized as common causes of disease. For example, inherited renal disorders, such as polycystic kidney disease and nephronophthisis, are now understood to be ciliopathies (Hildebrandt and Otto, 2005). Ciliary defects are also seen as the underlying cause of a number of inherited disorders that affect multiple organ systems. This helps explain the connection of retinal degeneration to ciliopathies, such as Bardet-Biedl syndrome (BBS), in which RP is found in association with multiple cilia-related disorders, including cystic renal disease, polydactyly, mental retardation, obesity and diabetes, gonadal malformations, and situs inversus (Satir and Christensen, 2007).

Ciliogenesis involves intraflagellar transport (IFT), which mediates the delivery of ciliary components to the growing ciliary tip, the point at which new cilium assembly occurs. The transported materials include tubulin subunits, tubulin-associated proteins, cell surface receptors, and other membrane proteins. IFT proteins have been biochemically characterized in *Chlamydomonas* as two complexes associated with anterograde (complex B) or retrograde (complex A) transport (Cole *et al.*, 1998). Mutations in IFT complexes and other ciliary component genes have been identified in numerous ciliopathies (Pierce *et al.*, 1999; Lehman *et al.*, 2008; Louie *et al.*, 2010; Muller *et al.*, 2010; Davis *et al.*, 2011).

The pleiotropic phenotypes of ciliary disorders suggest the involvement of genes having a highly conserved, essential function in the formation and/or maintenance of cilia. The inheritance patterns of ciliopathies are mostly autosomal recessive, but with extensive genetic heterogeneity (Badano *et al.*, 2006). The ciliopathy-related mutations identified so far affect proteins residing in the basal body, transition zone, ciliary membrane, IFT, or BBSome complexes. More loci are likely to be identified.

Although some progress has been made in the characterization of IFT complexes and BBSome proteins, proteomic studies of several model systems indicate many proteins are expressed in cilia (Ostrowski *et al.*, 2002; Keller *et al.*, 2005; Pazour *et al.*, 2005; Liu *et al.*, 2007; Mayer *et al.*, 2009; Jia *et al.*, 2010). For example, we identified nearly 2000 proteins in PSC in proteomic analyses of mouse PSCs (Liu *et al.*, 2007). These data suggest ciliogenesis is a complicated process and many uncharacterized proteins are involved.

In the work reported here, we have evaluated the role of a novel cilia protein Ttc26, which we detected in the mouse PSC proteome (Liu *et al.*, 2007). Ttc26 has been classified as an IFT complex B protein based on in vitro coprecipitation with Ift88 (Follit *et al.*, 2009). In addition, the *Caenorhabditis elegans* homologue of Ttc26, called dyf-13, is proposed to interact with OSM-3, a homodimeric kinesin motor, to move cargo in the anterograde direction during IFT (Starich *et al.*, 1995; Blacque *et al.*, 2005). In its N-terminal portion, Ttc26 contains several tetratricopeptide repeats (TPR). The TPR motif is enriched in the ciliary proteome and may mediate its interaction with other ciliary proteins in higher-order complexes. Notably, mutations in proteins with multiple TPRs, such as fleer/DYF-1, BBS4, BBS8, and TTC21B have been reported as ciliopathy-causing genes either in animal models or in human patients (Katsanis *et al.*, 2002; Pathak *et al.*, 2007; Harville *et al.*, 2010; Riazuddin *et al.*, 2010; Davis *et al.*, 2011). The studies reported here demonstrate that Ttc26 is located in the transition zone of primary and photoreceptor cilia and is required for normal ciliogenesis in cultured cells and in vivo in zebrafish.

RESULTS

Ttc26 is a highly conserved protein expressed in tissues containing ciliated cells

We detected Ttc26 as a novel PSC protein in our proteomic analyses of PSCs isolated from mouse retina. In those analyses, Ttc26 was detected by eight unique peptides, suggesting that it is present in moderate abundance in mouse PSCs (Liu *et al.*, 2007). To get an indication of the evolutionary importance of Ttc26, we searched the National Center for Biotechnology Information protein sequence database and found homologues from green algae, insects, and mammals. Alignment of Ttc26 homologue protein sequences from species related to the current study (CLUSTAL W method; Supplemental Figure S1) revealed very high sequence conservation (humans and rodents: 97% identity, 99% similarity; zebrafish and humans/rodents: 80% identity, 90% similarity). Ttc26 is highly conserved across the species we examined. The sequence conservation is observed throughout the protein, not just in TPR domains.

We used northern blots to determine which mouse tissues express transcripts of *Ttc26* and how abundant the transcripts are. In testis, which displayed the highest expression level, two different-sized transcripts were identified (Figure 1A). The larger transcript (4.2 kb) is consistent with the largest splice variant annotated in Ensembl (ENSMUST00000162554; CCDS51750) and was also detected in mouse retina, kidney, lung, and brain tissue. The expression level was low in liver and spleen, consistent with the low proportion of ciliated cells in these tissues (Figure 1A). The smaller transcript (2.5 kb) may represent an alternative splice variant in testis and is consistent with Ensembl transcript ENSMUST00000039394, in which exons 7–17 of the larger transcript are skipped. We also examined *ttc26* developmental expression in embryonic zebrafish and found that *ttc26* transcripts can be detected as early as the one-cell stage (possibly reflecting both maternal and embryonic contributions) and maintain a relatively stable level during the examined developmental stages (Figure 1B).

Ttc26 is localized in the transition zone of primary and photoreceptor sensory cilia

After confirming the temporal and spatial sequence of Ttc26 expression, we examined its subcellular localization by expressing a V5-tagged mouse Ttc26 fusion protein in murine inner medullary collecting duct 3 cells–somatostatin receptor 3–enhanced green fluorescent protein (mIMCD3-SSTR3-EGFP) cells. This stable cell line, derived from medullary collecting duct cells, expresses a green fluorescent protein (GFP) fused to SSTR3, a ciliary membrane receptor. By performing colocalization of Ttc26 with this ciliary marker, we showed that Ttc26 was concentrated in the ciliary base with gradually decreasing staining intensity toward the ciliary tip in interphase cells (Figure 1C). By immunostaining with antibodies to CEP164, a basal body distal appendage marker protein (Graser *et al.*, 2007), we refined the Ttc26 subcellular location at the base to the ciliary transition zone. Interestingly, Ttc26 does not localize to the distal appendage itself, but rather lies immediately adjacent to it. However, the punctate signal spreading in whole cilia (Figure 1C) suggests that Ttc26 is not restricted to the transition zone and is possibly mobile in a protein complex.

We also studied Ttc26 subcellular location in neonatal rat photoreceptor cells using an in vivo retinal electroporation approach to

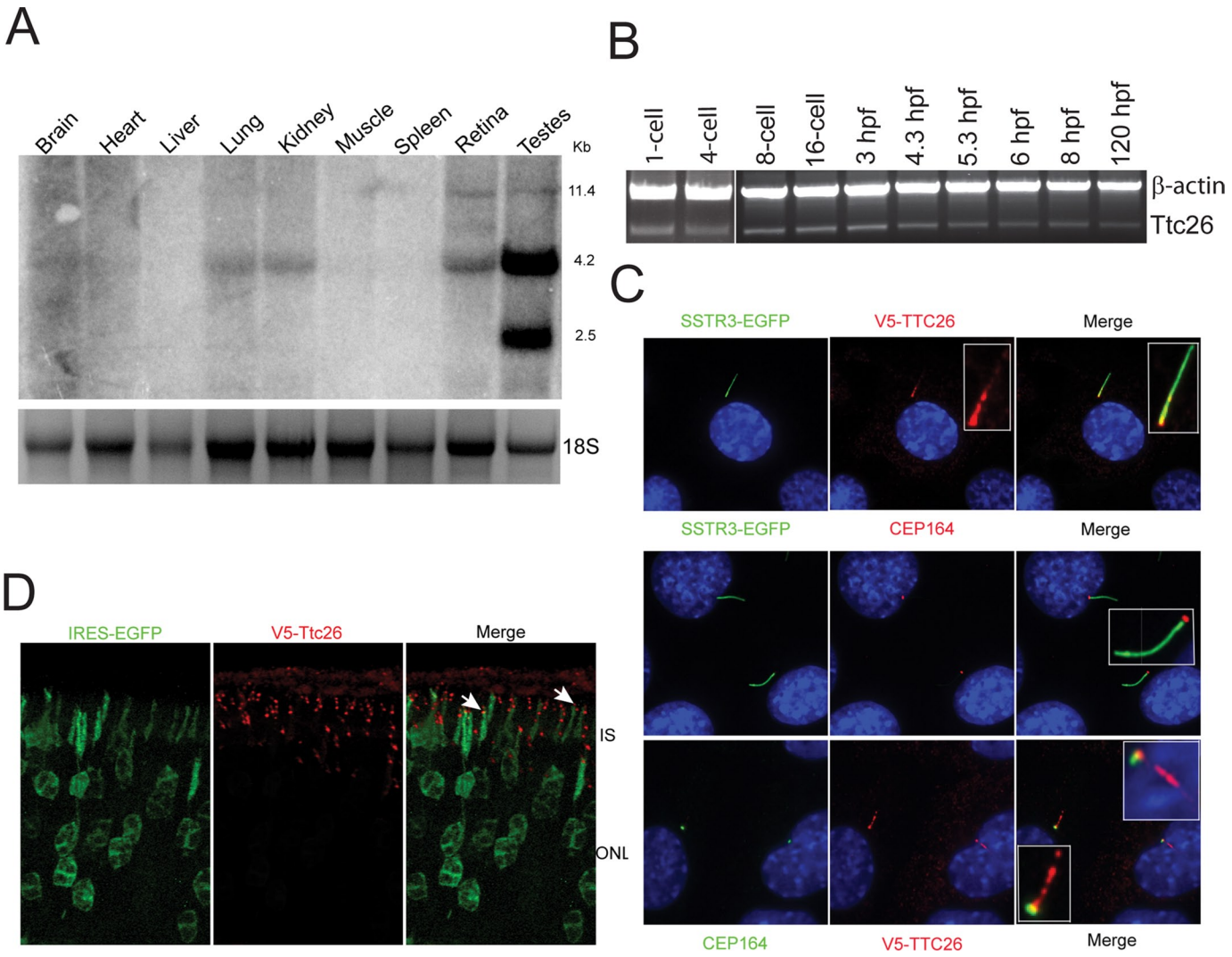

FIGURE 1: Expression of Ttc26 in cultured mIMCD3 cells, rodent tissues, and zebrafish embryos. (A) Northern blot of *Ttc26* in adult mouse tissues. *Ttc26* expression is high in the testis, with a 2.5-kb transcript exclusively seen in testis and a 4.2-kb transcript detected in testis, brain, heart, lung, kidney, and retina. The 11.4-kb band may represent unprocessed RNA. (B) Developmental expression of *ttc26* in zebrafish embryos. RT-PCR data revealed *ttc26* transcription was active at the one-cell stage and maintained at a relatively stable level through the developmental process (note that samples of one-cell and four-cell embryos were not loaded on the same gel). (C) Top, V5-Ttc26 fusion protein (red) colocalized with cilia (green) in SSTR3-EGFP-mIMCD3 cells. Ttc26 protein is most concentrated in the ciliary base. Middle, Cep164 (red), a distal appendage protein in basal body, is expressed in cilia (green) of SSTR3-EGFP-mIMCD3 cells. Bottom, V5-Ttc26 protein is partially overlapped with Cep164 in the basal bodies of mIMCD3 cells. Right, merged images. Note that the two proteins locate closely but not overlap. Insets, enlarged images of the cilia. (D) Neonatal rat photoreceptor cells transfected by in vivo electroporation with the plasmid pCAG-V5-*Ttc26*-IRES-EGFP are revealed by IRES-EGFP expression (green). Ttc26 recombinant protein, detected by immunostaining of the V5 tag, is localized to the transition zone of the transfected photoreceptor cells (red, arrows) on the top of the inner segments filled with water-soluble EGFP. Right, merged images.

transfect the same plasmid DNA used in the mIMCD3 cell transfection. Using immunostaining to the V5 tag on the Ttc26 fusion protein, we were able to localize Ttc26 to the transition zone in photoreceptor cells (Figure 1D) and thus confirm it as a bona fide ciliary protein.

RNA interference (RNAi) knockdown of *Ttc26* causes a defect in primary cilia in cultured kidney epithelial cells

The identification of Ttc26 as a transition zone protein suggests that it may play a functional role in ciliogenesis. To test this hypothesis, we used a ciliated renal epithelial cell model (mIMCD3) in vitro to study the effects of knockdown of *Ttc26* expression. Three short hairpin RNA (shRNA) constructs directed at *Ttc26* were introduced into target cells using a vector expressing GFP (pCAG-miR30-IRES-EGFP). This allowed us to identify all shRNA-transfected cells. Cotransfection of these *Ttc26* shRNAs with the V5-*Ttc26* cDNA in CHO cells demonstrated that all three shRNA constructs had knockdown efficiencies of over 90% compared with control shRNAs (Figure 2A). Next we tested the effect of shRNA-mediated *Ttc26* knockdown on ciliogenesis in mIMCD3 cells. In this case, cilia were detected by immunostaining with antibody to acetylated α-tubulin, an axoneme marker. Transfected mIMCD3 cells (green) were

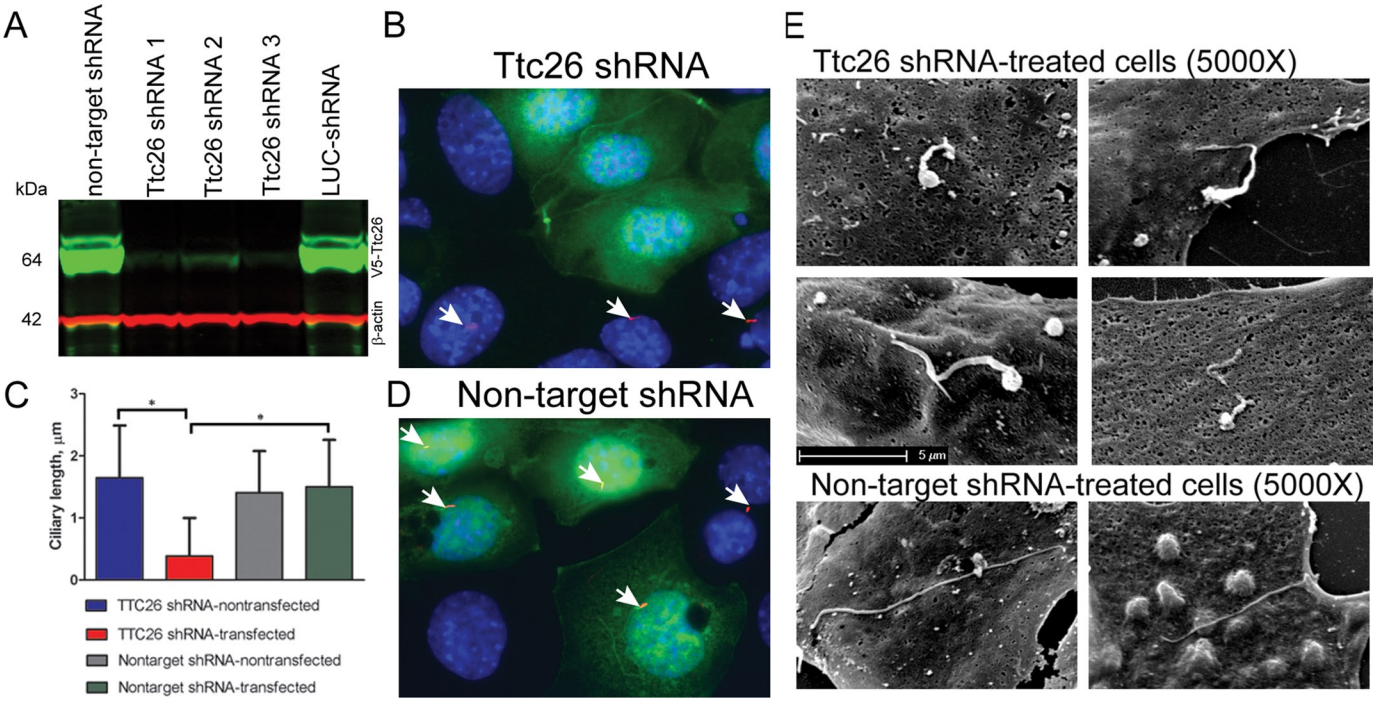

FIGURE 2: Knockdown of *Ttc26* by shRNA caused shortened cilia with altered morphology in mIMCD3 cells. (A) An immunoblot assay using anti-V5 antibody verified knockdown of expressed V5-*Ttc26* cotransfected with shRNA constructs in CHO cells. All three *Ttc26* shRNA constructs showed efficient knockdown of the V5-*Ttc26* transcript as compared with two control shRNA constructs. (B) Immunofluorescence image showing cilia (red) detected immunostaining for acetylated α-tubulin in mIMCD3 cells transfected with *Ttc26* shRNA (green) and in nontransfected cells. (C) Quantification of *Ttc26* knockdown effects on ciliary length. Error bars represent SDs between three independent experiments ($n = 829$ for *Ttc26* shRNA-transfected or nontransfected cells; $n = 275$ for control shRNA-transfected and nontransfected cells; *, $p < 0.01$ by t test). (D) Cells transfected with nontarget control shRNA exhibit green fluorescence but do not show the effects of *Ttc26* knockdown (arrows point to cilia in B and D). (E) Scanning electron micrographs of mIMCD3 cells treated with *Ttc26* shRNA or nontarget control shRNA. Defective cilia were identified as being shortened with enlarged ends compared with the long and slender cilia in cells treated with control shRNA.

observed to have shortened cilia or missing cilia (arrows in Figure 2B). We further analyzed the images by quantifying the number of transfected cells with and without cilia and by measuring the ciliary length in both transfected cells and adjacent nontransfected cells. Using this approach, we found that knockdown of *Ttc26* was associated with significantly reduced ciliary length ($p < 0.01$; Figure 2, B and C). Nontransfected mIMCD3 cells are shown for comparison in Figure 2D. To investigate the effects of *Ttc26* knockdown on ciliary morphology, we examined shRNA-transfected and nontransfected mIMCD3 cells by scanning electron microscopy (SEM) and observed that cells with *Ttc26* knockdown displayed shortened cilia with enlarged ends (Figure 2E).

Morpholino knockdown of *ttc26* disrupts photoreceptor outer segment morphogenesis in developing retina

To further assess the functional importance of Ttc26, we turned to a vertebrate model organism, the zebrafish. Over a period of 2 d, the optic cup transforms from a single neuroepithelial sheet into a functional multilayered retina (Fadool and Dowling, 2008). This makes it particularly suitable for a developmental study of photoreceptor cell morphogenesis. We used knockdown by two *ttc26* morpholino oligonucleotides (MO-AUG and MO-SP) to further test the hypothesis that ttc26 functions in ciliogenesis. The MO-AUG and MO-SP morpholinos were designed to interfere with translation initiation and RNA splicing, respectively. The MO-SP blocks splicing between exons 1 and 2, leading to the inclusion of intron 1 in the altered mRNA transcript. This introduces a premature termination codon 20 nucleotides into intron 1, which leads to a truncated protein and loss of function. Molecular analysis of reverse transcription PCR (RT-PCR) products from embryos injected with MO-SP revealed mis-splicing events (Figure 3, D and E) consistent with a loss-of-function phenotype similar to that caused by MO-AUG.

Embryos injected with a control morpholino were normal in appearance (Figure 3A, 1 and 2). However, the morphant larvae exhibited body axis curvature (mostly ventral and sometimes dorsal) and kinked tails (Figure 3A, 3–10). The MO-AUG and MO-SP morpholinos led to very similar phenotypes in appearance and in histology, except the MO-SP morphants also displayed severe body edema.

The histology of 5 d postfertilization (dpf) zebrafish eye morphogenesis in control and *ttc26* morphants is presented in Figure 3B. At higher magnification (60×), the five principal laminae—three cellular and two plexiform layers—can be seen to be fully formed in the retinas of both control and morphant larvae, and the proliferative marginal zones (MZ) developed normally and remained nonlaminated in both controls and morphants. A higher-magnification view of the control retina shows clear morphological differentiation of photoreceptors with well-defined inner and outer segments at 5 dpf (Figure 3B). In contrast, both types of morphants revealed a defective photoreceptor ciliogenesis with only a few outer segments visible. Outer segments in these retinas were smaller, shortened, and disorganized.

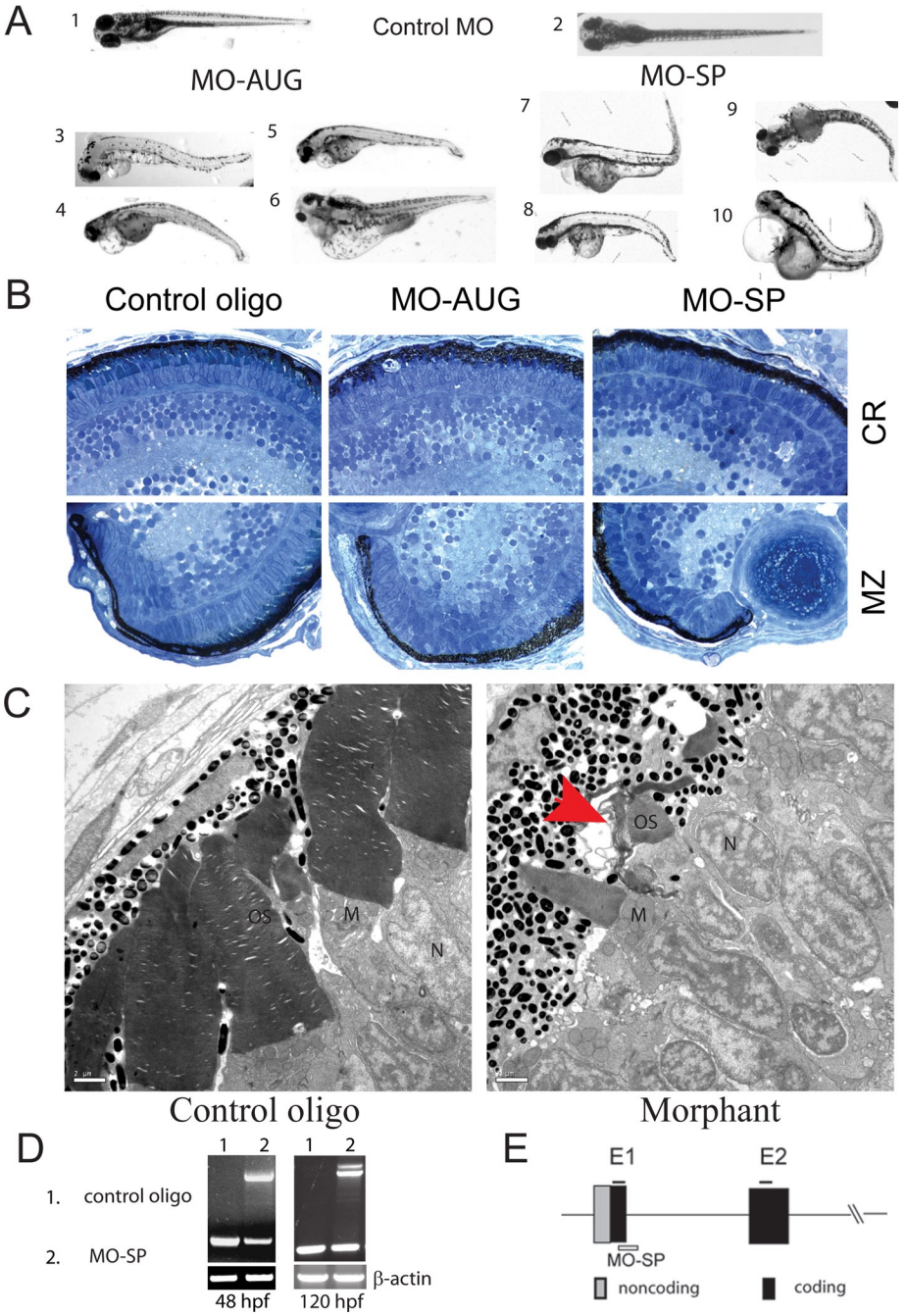

FIGURE 3: Phenotypes of *ttc26* zebrafish morphant larvae. Zebrafish embryos were injected with two *ttc26* MOs (MO-AUG and MO-SP) or control MO. (A) Knockdown of *ttc26* results in developmental defects. Panel 1, lateral view of 120-hpf larva injected with control MO. Panel 2, dorsal view of the control MO-treated larva. Panels 3–6, lateral views of 120-hpf morphant larvae injected with *ttc26* morpholino MO-AUG. The *ttc26* morphants displayed curled or kinked tails, precardiac edema, and shortening of the body. Panels 7–10, dorsal or lateral view of 72-hpf morphant larvae injected with *ttc26* morpholino MO-SP. The curled or kinked tails and body curvature are very similar to those of MO-AUG morphants. (B) Eye morphology is altered in *ttc26* morphants at 5 dpf. Histological sections are shown for eyes, central retina (CR), and retinal marginal zone (MZ) from larvae injected with control MO and *ttc26* MO-AUG. Left, retina of 5-dpf fish injected with the control MO display well-formed laminae (top), with details visible in high magnification (60×) views of the central retina (CR, middle) and marginal zone (MZ, bottom). The higher magnification (60×) views of the morphant retinas reveal shortened and disorganized photoreceptor outer segments in the retina, with otherwise normal lamination. (C) TEM of the control-MO larvae at 5 dpf shows normally developed photoreceptor outer segments with densely packed disks (left). TEM of the morphant larvae shows that outer segments are smaller, shortened, and disoriented (right), consistent with the morphology seen in the light micrographs in (B). Note that a disorganized partial outer segment can be seen on the left adjacent to a cone photoreceptor (red arrow). N, nucleus; M, mitochondria; OS, outer segment. (D) RT-PCR analyses confirm that morpholino MO-SP interferes with splicing of *ttc26* mRNA in larvae. Forty-eight hours postfertilization and 120-hpf larvae injected with control-MO or MO-SP were used for RNA extraction and RT-PCR. The lower band (590 base pairs) visible in both conditions represents PCR product from correctly spliced mRNA. The larger PCR product (1553 base pairs, containing the 963–base pair nonsplicing intron 1) is detected after MO-SP treatment due to the blocked splice donor site. As shown, although not complete, splice blocking is more evident at 48 hpf, consistent with some recovery from the morpholino effect at 120 hpf. (E) The binding positions of the PCR primers (above) and the MO-SP oligo (below) are illustrated in a diagram. For simplicity, only exons 1 and 2 are shown.

Transmission electron microscopy (TEM) images of the controls show well-formed photoreceptor outer segments. In contrast, morphant eyes reveal missing and ill-formed outer segments (Figure 3C).

MO-knockdown of *ttc26* results in dilated pronephric tube and duct

The observation of edema in *ttc26* morphants prompted us to look at the pronephros, the embryonic kidney, of zebrafish larvae for possible defects in fluid flow and in biogenesis of cilia, including motile cilia. Indeed, as shown in Figure 4, we found that morpholino knockdown of *ttc26* was associated with defects in cilia in the pronephros as early as 27 h postfertilization (hpf), with disrupted and disorganized cilia (Figure 4A). Video images taken at 2 dpf clearly show enlarged pronephric ducts and disruption of multiciliated-cell cilia beat coordination (Supplemental Movies S1, S2, and S3). The recorded video data showed the multiciliated-cell cilia beat coordination is disrupted. The overall beat rates increase from 34 beats per second (bps; control) to ~60 bps (morphants), most likely due to tubule lumen dilation (Hellman *et al.*, 2010; Figure 5). The distended and dilated pronephric tubules/ducts were observed in many morphants that exhibited precardiac and body edema at 5 dpf (Figure 4, C–E).

The finding that both the MO-AUG and MO-SP morpholinos produced the same phenotypes in both eyes and pronephric kidney supports the conclusion that these results are due to genuine *ttc26* knockdown and not to an off-target effect. To confirm

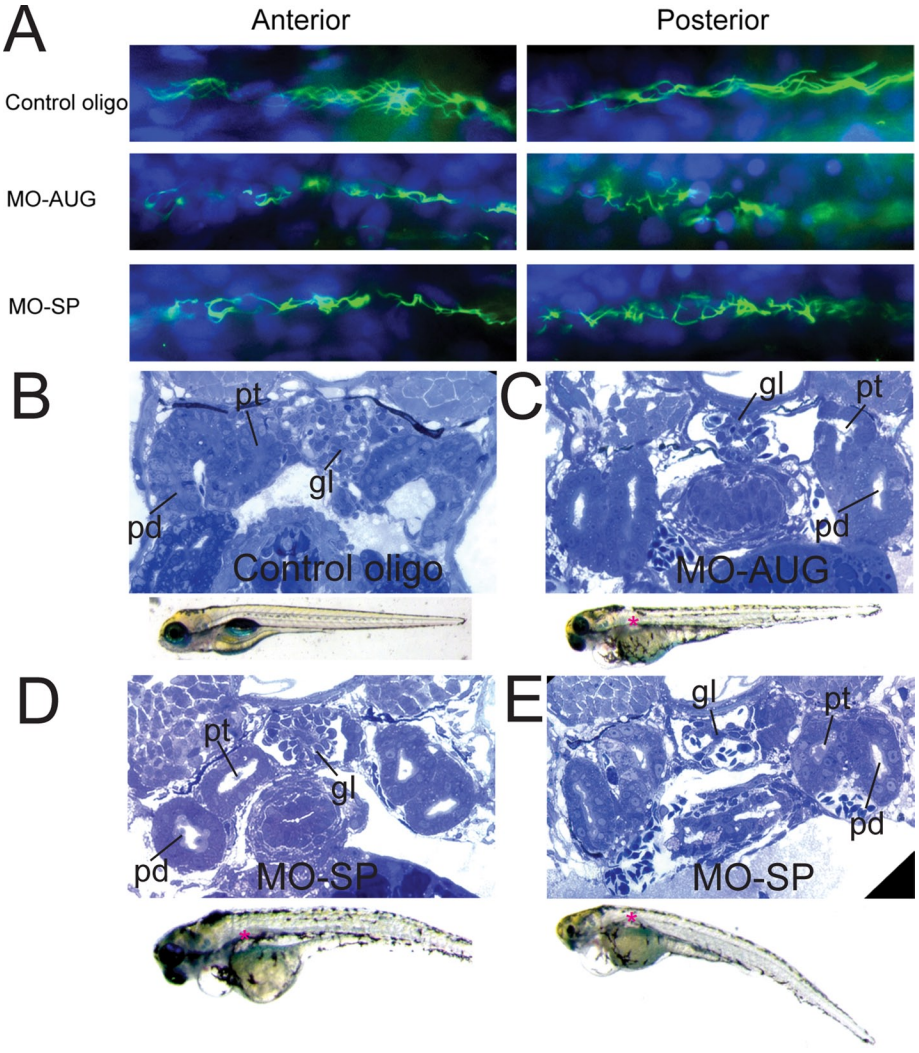

FIGURE 4: Morpholino knockdown of *ttc26* disrupts motile cilia and causes tubule dilation in zebrafish pronephros. (A) Cilia in the anterior and posterior regions of the pronephric kidneys in larvae at 27 hpf. Green, cilia revealed by immunostaining of acetylated α-tubulin; blue, nuclei. Top, cilia are long and well-organized in larvae injected with the control MO oligo. Middle and bottom, knockdown of *ttc26* by transfection with MO-AUG or MO-SP morpholinos leads to shortened, disorganized, and disoriented cilia. (B) Kidney cross-section in a 5-dpf larva shows normal morphology after injection with control–MO (C–E) Injection with MO-AUG or MO-SP morpholino leads to distended/dilated pronephric tubes and ducts. The zebrafish larvae used are shown below the corresponding micrograph images, with the defects marked (*). gl, glomerulus; pt, pronephric tubule; pd, pronephric duct.

that the morphological effects in zebrafish larvae were indeed associated with knockdown of *ttc26*, we used RT-PCR analysis to analyze the mRNA present in control and morphant larvae. Morpholino MO-SP treatment of zebrafish larvae partially blocks splicing of *ttc26* mRNA, and thus leads to a larger-sized PCR product (Figure 3, D and E). To further demonstrate the specificity of the MO-induced knockdown phenotypes, we performed rescue experiments with coinjection of *ttc26*-MO and *Ttc26* mRNA. Coinjection of 66 ng of mouse *Ttc26* mRNA with MO-AUG reduced the percentage of abnormal larvae from 95% (21/22) in the embryos injected with MO-AUG alone to 51% (23/45) in the coinjected embryos ($p < 0.001$).

DISCUSSION

The data presented here indicate that Ttc26 is localized to cilia in both mouse and rat cells and is developmentally required for ciliogenesis in zebrafish photoreceptor cells and pronephric kidney. Ttc26 is localized in the primary cilia and enriched in the transition zone of the mIMCD3 and rodent photoreceptor cells. Knockdown of *Ttc26* in mIMCD3 cells produced shortened and defective cilia. Furthermore, morpholino knockdown of *ttc26* in zebrafish caused larvae to exhibit absent or deformed photoreceptor outer segments, but with normal lamination in the morphant retina. The morphant larvae also developed defective motile cilia in the pronephros. These morphant phenotypes demonstrate that ttc26 is required for ciliogenesis and normal ciliary function.

Related genes involved in ciliary defects

The highly conserved polypeptide sequence of Ttc26, both within its TPR domains and in other regions, suggests an important function for this protein. Furthermore, *ttc26* knockdown in the eye and pronephros led to phenotypes that match those observed with defects in other ciliary genes in zebrafish larvae. These include body curvature, cardiac edema, pronephric distention and dilation, and photoreceptor outer segment defects (Malicki *et al.*, 2011). The overlap in phenotypes implies that ttc26 might function similarly to other TPR domain proteins found in ciliary protein complexes.

Ciliopathy-causal mutations have been identified in several TPR domain-containing genes, including *BBS4*, *BBS8*, *TTC21B*, and *TTC30B* (Katsanis *et al.*, 2002; Billingsley *et al.*, 2010; May-Simera *et al.*, 2010; Riazuddin *et al.*, 2010; Davis *et al.*, 2011). BBS4 and BBS8 are key scaffold components of the BBSome ciliary protein transport complex. TTC21B has been localized to centrosomes and is required for retrograde IFT, and causal mutations have been identified in human patients (Davis *et al.*, 2011). Fleer/dyf-1/TTC30B is a regulator of ciliary tubulin polyglutamylation. Mutants in *fleer* showed kidney cysts, randomized left–right asymmetry, hydrocephalus, and rod outer segment defects in zebrafish (Pathak *et al.*, 2007).

Photoreceptor outer segments

The outer segments or PSCs of photoreceptor cells require continuous transport of membrane and protein components due to the constant shedding and phagocytosis by retinal pigment epithelium cells of older disks at the distal ends of PSCs (Strauss, 2005). Protein trafficking mediated by IFT via the transition zone is crucial for the biogenesis and maintenance of the outer segment. This makes the transition zone an important "gate" in photoreceptor cells. Indeed, numerous mutations that cause IRDs and other ciliopathies, among them *RPGR, RPGRIP1*, and *TTC21B*, have been identified in genes of transition zone components (Vervoort *et al.*, 2000; Dryja *et al.*, 2001; Davis *et al.*, 2011).

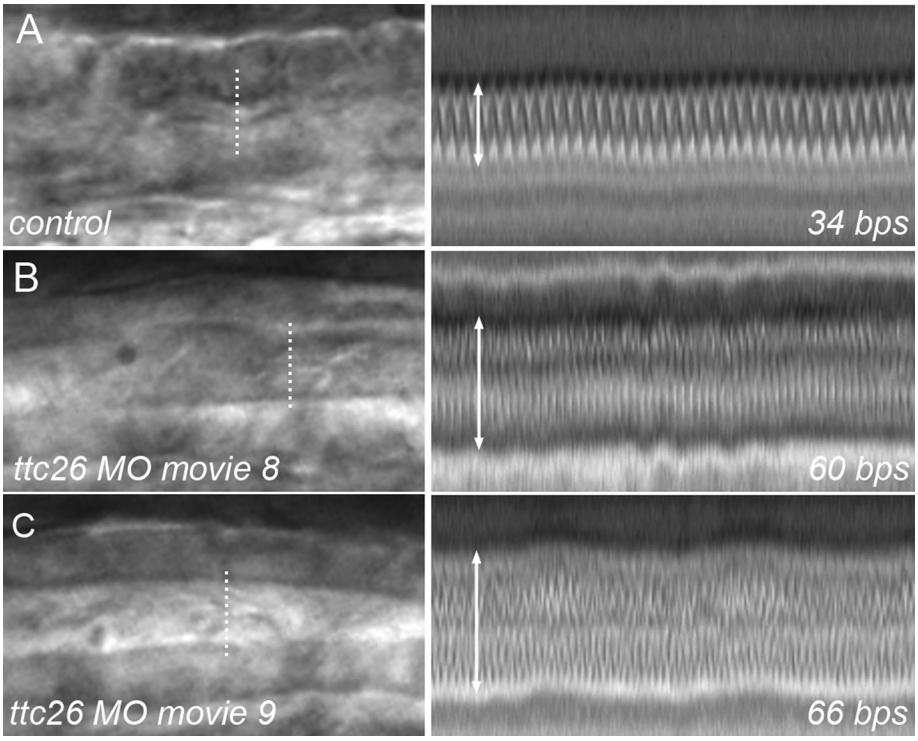

FIGURE 5: *ttc26* knockdown disrupts pronephric cilia beat coordination in 2-dpf larvae. Video images on the left show the dilated pronephros ducts in *ttc26* morphants (B and C) vs. control (A). Dotted lines, position of the line scan. Corresponding cilia beat amplitude line scans are shown on the right. Control cilia bundles beat coordinately, but the cilia beat rate in *ttc26* morphants (B and C) is increased and out of phase, resulting in loss of coordination. (See supplemental movies.)

Zebrafish morphants lacking *ttc26* are viable at least to the 5-dpf stage and show photoreceptor cells with short or missing PSCs. The loss of *ttc26* appears to prevent or delay PSC formation during early photoreceptor cell differentiation. While outer segment disk material is generated in some photoreceptor cells, it does not appear that this can be organized into formed PSCs in most photoreceptor cells. Although the morphant photoreceptor cells displayed defects in PSC formation, they maintained the ability to laminate and differentiate normally in the retina.

Relation of kidney defects to ciliopathy and ttc26 function

A hallmark of many human ciliopathies is the formation of kidney cysts, which often begins during fetal development. The observation of edema in zebrafish *ttc26* morphants prompted us to look for defects in cilia early in pronephros at 27 hpf. The kidney is a vital organ controlling homeostasis of water and electrolytes, osmoregulation of body fluids, and filtration of toxic metabolic waste products. Cilia in zebrafish pronephros have been reported to be motile and to drive fluid flow (Kramer-Zucker *et al.*, 2005). Therefore disruption of the cilia would logically be accompanied by a loss of fluid flow, leading to fluid accumulation and subsequent pronephric distension and dilation. As expected, *ttc26* morphant larvae at 27 hpf exhibited disorganized and disrupted cilia, loss of cilia bundles in the pronephric duct, and distended pronephric tubules and ducts, and this would logically contribute to the disruption of kidney function and severe edema observed in zebrafish larvae after *ttc26* knockdown.

In summary, our characterization of Ttc26 localization and function in mouse and rat tissue, mIMCD3 cells, and in zebrafish provides the first comprehensive studies of *Ttc26* gene expression and function in primary and sensory cilia. This work demonstrates that Ttc26 plays a critical role in ciliogenesis and suggests that loss of Ttc26 function could be implicated in retinal, renal, and other disease states in humans. Further studies confirming and extending these findings in other species will help us to better understand the function of Ttc26 in cilia. In this light, it seems logical to screen human patient populations with ciliopathies for mutations of *TTC26* and genes that encode other ciliary proteins involved in IFT.

MATERIALS AND METHODS

Gene expression reagents

Mouse *Ttc26* cDNA was amplified by RT-PCR from mouse retina, cloned into a pENTR/D-TOPO entry vector (Invitrogen, Carlsbad, CA), and fully sequence-verified. The coding sequence was moved by recombination to a Gateway destination expression vector modified to contain an N-terminal V5 epitope tag in-frame (pCAG-V5-IRES-EGFP; Hartley *et al.*, 2000; Matsuda and Cepko, 2004, 2007). The sequences of shRNA knockdown reagents were generated using the RNAi Central website (Cold Spring Harbor, http://hannonlab.cshl.edu). Oligonucleotides of shRNA (obtained from IDT, Coralville, IA) were PCR-amplified and cloned into a pCAG-miR30-IRES-EGFP vector, modified by our laboratory for this purpose using established methods (Hartong *et al.*, 2006). Plasmid DNA was purified using the EndoFree Plasmid Maxi kit (Qiagen, Valencia, CA).

Cell culture and transfection

An mIMCD3 stable cell line expressing SSTR3-EGFP, a ciliary membrane marker (gift of Gregory J. Pazour, University of Massachusetts Medical School), was used for Ttc26 subcellular localization. CHO-K1 and wild-type mIMCD3 cell lines were purchased from the American Type Culture Collection. The mIMCD3 cells were maintained in DMEM:F12 media supplemented with 10% fetal bovine serum (FBS) and 0.5 mM sodium pyruvate (Invitrogen). CHO cell culture was performed in F-12K medium (Invitrogen) supplemented with 10% FBS. Transfection was performed with Lipofectamine 2000 or Lipofectamine LTX reagent (Invitrogen) using 4 μg DNA per well and cells at 60–70% confluency in a six-well plate with glass coverslips (25CIR-1D; Fisher, Pittsburgh, PA). The cells were processed for immunocytochemistry at 72 h after transfection. Detection of the recombinant protein fused to the V5 epitope tag was accomplished by immunocytochemical detection or immunoblot of the V5 tag.

Antibody reagents

Monoclonal antibody (mAb) against acetylated α-tubulin (clone 6-11B-1) was obtained from Sigma-Aldrich (St. Louis, MO) and anti-V5 tag mAb from Invitrogen. Anti-CEP164 antibody (human), recognizing a basal body distal appendage marker protein, was a gift (Graser *et al.*, 2007). Anti–β-actin antibody (C-11) was purchased from Santa Cruz Biotechnology (Santa Cruz, CA). All secondary antibodies conjugated with fluorophores were from Invitrogen, except the antibody used for immunoblot, which was obtained

from LI-COR (Lincoln, NE). The chemical reagents were purchased from Sigma-Aldrich.

Immunofluorescence microscopy

All incubations and washes were carried out in 1× phosphate-buffered saline (PBS) at room temperature. Cells were fixed in 4% paraformaldehyde for 10 min, permeabilized with 0.5% Triton X-100 in PBS for 10 min, and blocked with 1% bovine serum albumin (BSA) and 0.2% Triton X-100 in PBS for 10 min. Next the cells were incubated with antibody to the V5 expression tag (1:2500 dilution) in blocking buffer for 1 h at room temperature. After three 10-min washes in PBS, a secondary antibody incubation was carried out for 1 h in Alexa Fluor 555–conjugated goat anti–mouse immunoglobulin G (IgG; 1:1000 dilution). The cells were then washed once in PBS for 10 min, incubated with Hoechst dye (Invitrogen) at 1:1000 dilution for 5 min, and washed twice (10 min each wash). For colocalization to the basal body, cells were incubated using the above procedure with antibody against human CEP164 for 1 h (1:1000 dilution) and Alexa Fluor–conjugated goat anti–mouse IgG (1:1000 dilution; Invitrogen) for 1 h. The coverslips were mounted using Fluoromount (Electron Microscopy Sciences, Hatfield, PA). Fluorescence signals were visualized using a Nikon TE300 fluorescence microscope.

In vivo electroporation

To localize Ttc26 expression in photoreceptor cells, we used an in vivo electroporation technique in rat photoreceptor cells. Briefly, 0.5 µl of endotoxin-free pCAG-V5-*Ttc26*-IRES-EGFP plasmid was injected subretinally into the right eyes of neonatal rats. Injected plasmid was electroporated into retinal cells using tweezer-type electrodes as previously described (Matsuda and Cepko, 2004). The plasmid was injected into four to six eyes to provide sufficient retinas with both good transfection and morphology for analysis. Animals were killed 4 wk following injection, and frozen sections were prepared from the portions of the eyecups with EGFP signal. Sections were immunostained as described previously using anti-V5 antibody followed by Alexa Fluor 555–conjugated secondary antibody. The location of V5-tagged proteins in photoreceptor cells was evaluated by three-dimensional reconstructions of the confocal image stacks generated and analyzed using Volocity 3D imaging software (Mountain View, CA).

Northern blot and immunoblot analyses

RNA expression levels were analyzed by northern blot analysis. To prepare a cDNA probe for northern blot analysis, we cloned the full-length mouse *Ttc26* cDNA (NM_153600) into a pCR2-TOPO vector. The plasmid was digested with *Eco*RI, and the insert DNA was purified using the QIAEX II gel extraction kit (Qiagen). Northern blot analysis was performed as described previously (Zhang *et al.*, 2000). Briefly, total RNA (25 µg) was extracted with TRIzol reagent (Invitrogen), separated on a 1% agarose/0.66 M formaldehyde gel, and transferred to a Gene Screen *Plus* nylon membrane (Perkin Elmer-Cetus, Waltham, MA) by capillary blotting for 24 h in 10× SSC. The probe was labeled with α-dCTP (deoxycytidine triphosphate)-[^{32}P] and hybridized with the RNA blot at 10^6 cpm/ml of hybridization buffer. The blots contained multiple tissues, including retinas from a wild-type adult mouse. For this reason, after decay of the cDNA probe signals, the membranes were rehybridized with an [α^{32}P]-labeled cDNA probe for 18S RNA to assess and normalize RNA sample loading. The signal was scanned using a Typhoon 9400 phosphorimager (GE, Waukesha, WI).

Immunoblot analysis was used to verify knockdown of gene constructs expressed in CHO cells. Cells were transfected with pCAG V5-*Ttc26*-IRES-EGFP plasmid DNA (4 µg well) in a six-well plate. At 48 h after transfection, the plate was rinsed twice with cold 1× PBS and then the cells were lysed immediately with 2× LDS sample buffer (Invitrogen) and sonicated briefly on ice. Total protein (100 µg/well) was separated on a precast NuPAGE 4–12% Bis-Tris Gel (Invitrogen) and transferred to a low-fluorescence polyvinylidene fluoride membrane (GE, Waukesha, WI). The membrane was incubated with Odyssey blocking buffer (LI-COR, Lincoln, NE) for 1 h at room temperature. The membrane was incubated with monoclonal anti-V5 antibody (1:5000 dilution) overnight with gentle rocking in a cold room, washed 4 times with 1× PBS with 0.1% Tween-20, incubated with IRDye (LI-COR) goat anti-mouse IgG (1:10,000 dilution) for 1 h at room temperature, and washed three times with PBS with 0.1% Tween-20. After a final wash with 1× PBS, the signals were detected with an Odyssey infrared imager (LI-COR). The loading control antibody to β-actin was used at 1:1000. Protein levels (expressed in fluorescence units) were quantified with software provided by LI-COR.

MOs and zebrafish embryo injection

Wild-type zebrafish (*Danio rerio*) of the AB strain were obtained from the University of Pennsylvania zebrafish core facility (Philadelphia, PA). Embryos were collected in E3 solution after natural spawns and kept at 28.5°C in an incubator using standard protocols (Westerfield, 2007). Morpholinos designed to block *ttc26* RNA translation (MO-AUG, 5′-CTGGCTTCATCCGAGACAAGAGCAT-3′) or to block splicing (MO-SP, 5′- ATATGTTGGTTCTGATGCACCTGTT-3′) and a standard control oligo (5′-CCTCTTACCTCAGTTACAATTTATA-3′) were obtained from Gene Tools (Philomath, OR).

Embryos were injected at the one- to two-cell stages with 0.35–0.45 mM MO (3.5–4.5 ng of ttc26 MO or 4.5 ng of control MO).

Embryos were imaged with a Stemi SV II stereomicroscope (Zeiss) and photographed with an AxioCam digital camera (Zeiss), and the images were analyzed with AxioVision software (Zeiss). Embryos were prepared for flat-mounting by dissecting the yolk away from the embryo proper with a pair of fine forceps; the embryos were then mounted between two glass coverslips. Immunofluorescence detection of acetylated tubulin in the whole-mount embryos was performed according to a published protocol (Jaffe *et al.*, 2010).

High-speed video microscopy analysis has been described in detail in a recent publication (Pathak *et al.*, 2011). Larvae at 2 dpf were used for the video recording.

RT-PCR

Whole embryos (both morphant and control) collected at different developmental stages were used for total RNA extraction with TRIzol reagent (Invitrogen). Total RNA (2 µg per sample) was reverse-transcribed using the Superscript first-strand synthesis system for RT-PCR (Invitrogen). The following primer pairs were used for RT-PCR. For *ttc26* developmental expression: forward, 5′-ATGCGCTCTCATTACCAGGAGGC-3′; reverse, 5′-AGAGGCCATGCACTGCCTGCCTGG-3′. For detecting morpholino splice blocking: forward (exon 1), 5′-CACCATGCTCTTGTCTCGGATGAAGC-3′, reverse (exon 2), 5′-GCCACATACACATTCAGGGCCAGAA-3′. For β-actin primers: forward, 5′-ATGGATGAGGAAATCGCTGCCCTG-3′; reverse, 5′-ACCGATCCAGACGGAGTATTTGCGC-3′.

For the phenotype rescue studies, mouse *Ttc26* cDNA was amplified by PCR with a pair of primers (forward, 5′-TGCGGCCCAGACTGGCGGACGCG-3′; reverse, 5′-ATGACAACTGAGACAGGCAAGCAGG-3′) and cloned into an Sp6/T7 promoter vector (pCS2P+; Addgene, Cambridge, MA). The plasmid was linearized with *Sna*BI. Capped Ttc26 mRNA was synthesized in vitro using the

mMESSAGE mMACHINE SP6 kit (Ambion, Austin, TX) and purified by the RNeasy Plus micro kit (Qiagen). Mouse *Ttc26* mRNA (5–17 pg) was coinjected with MO-AUG (0.35 ng) into one- to two-cell stage zebrafish embryos.

Histology and SEM and TEM

Zebrafish embryos were processed for histology and TEM following a Cold Spring Harbor Protocol (http://cshprotocols.cshlp.org/content/2007/6/pdb.prot4772.abstract). For general histology, transverse semithin sections (1 µm) were stained with alkaline Toluidine blue. For TEM, thin sections (90 nm) were mounted on electron microscopy grids and stained with lead citrate and uranyl acetate. TEM images were collected on a FEI-Tecnai T12 transmission electron microscope. For SEM, cultured cells were processed using standard protocols. Briefly, mIMCD3 cells grown on 13-mm coverslips were rinsed twice with PBS, washed three times with 50 mM Na-cacodylate buffer (pH 7.3), fixed for 2 h with 2% glutaraldehyde in 50 mM Na-cacodylate buffer, and dehydrated in a graded series of ethanol concentrations over a period of 1.5 h. Dehydration in 100% ethanol was done three times. The dehydrated samples were immersed twice for 10 min in 100% hexamethyldisilazane (HMDS; Sigma-Aldrich, St. Louis, MO), which was followed by air-drying for 30 min (Braet *et al.*, 1997). The samples were mounted on stubs and sputter-coated with gold palladium. Specimens were observed and photographed using a Philips XL20 scanning electron microscope (FEI, Hillsboro,OR) at 10-kV accelerating voltage.

Statistical analyses

Statistical analyses were performed with Minitab software. A Student's *t* test with unequal variance or chi-square test was used for the analyses.

ACKNOWLEDGMENTS

We thank Gregory Pazour for providing the SSTR-3 mIMCD3 cell line and Michael Pack and Jie He of the Zebrafish Core at Penn Medicine for their assistance. This work was supported by grants from the National Institutes of Health (R01-EY012910 to E.A.P.), the Foundation Fighting Blindness USA, the F. M. Kirby Foundation, Research to Prevent Blindness, and the Rosanne Silbermann Foundation. We also acknowledge the contribution of medical editing by David Titus.

REFERENCES

Badano JL, Mitsuma N, Beales PL, Katsanis N (2006). The ciliopathies: an emerging class of human genetic disorders. Annu Rev Genomics Hum Genet 7, 125–148.

Beisson J, Wright M (2003). Basal body/centriole assembly and continuity. Curr Opin Cell Biol 15, 96–104.

Billingsley G *et al.* (2010). Mutations in chaperonin-like BBS genes are a major contributor to disease development in a multiethnic Bardet-Biedl syndrome patient population. J Med Genet 47, 453–463.

Blacque OE *et al.* (2005). Functional genomics of the cilium, a sensory organelle. Curr Biol 15, 935–941.

Braet F, de ZR, Wisse E (1997). Drying cells for SEM, AFM and TEM by hexamethyldisilazane: a study on hepatic endothelial cells. J Microsc 186, 84–87.

Breunig JJ, Sarkisian MR, Arellano JI, Morozov YM, Ayoub AE, Sojitra S, Wang B, Flavell RA, Rakic P, Town T (2008). Primary cilia regulate hippocampal neurogenesis by mediating sonic hedgehog signaling. Proc Natl Acad Sci USA 105, 13127–13132.

Cole DG, Diener DR, Himelblau AL, Beech PL, Fuster JC, Rosenbaum JL (1998). *Chlamydomonas* kinesin-II-dependent intraflagellar transport (IFT): IFT particles contain proteins required for ciliary assembly in *Caenorhabditis elegans* sensory neurons. J Cell Biol 141, 993–1008.

Davis EE *et al.* (2011). TTC21B contributes both causal and modifying alleles across the ciliopathy spectrum. Nat Genet 43, 189–196.

Dryja TP, Adams SM, Grimsby JL, McGee TL, Hong DH, Li T, Andreasson S, Berson EL (2001). Null RPGRIP1 alleles in patients with Leber congenital amaurosis. Am J Hum Genet 68, 1295–1298.

Fadool JM, Dowling JE (2008). Zebrafish: a model system for the study of eye genetics. Prog Retin Eye Res 27, 89–110.

Follit JA, Xu F, Keady BT, Pazour GJ (2009). Characterization of mouse IFT complex B. Cell Motil Cytoskeleton 66, 457–468.

Graser S, Stierhof YD, Lavoie SB, Gassner OS, Lamla S, Le CM, Nigg EA (2007). Cep164, a novel centriole appendage protein required for primary cilium formation. J Cell Biol 179, 321–330.

Hartley JL, Temple GF, Brasch MA (2000). DNA cloning using in vitro site-specific recombination. Genome Res 10, 1788–1795.

Hartong DT, Berson EL, Dryja TP (2006). Retinitis pigmentosa. Lancet 368, 1795–1809.

Harville HM *et al.* (2010). Identification of 11 novel mutations in eight BBS genes by high-resolution homozygosity mapping. J Med Genet 47, 262–267.

Hellman NE, Liu Y, Merkel E, Austin C, Le CS, Beier DR, Sun Z, Sharma N, Yoder BK, Drummond IA (2010). The zebrafish foxj1a transcription factor regulates cilia function in response to injury and epithelial stretch. Proc Natl Acad Sci USA 107, 18499–18504.

Hildebrandt F, Otto E (2005). Cilia and centrosomes: a unifying pathogenic concept for cystic kidney disease? Nat Rev Genet 6, 928–940.

Horst CJ, Johnson LV, Besharse JC (1990). Transmembrane assemblage of the photoreceptor connecting cilium and motile cilium transition zone contain a common immunologic epitope. Cell Motil Cytoskeleton 17, 329–344.

Jaffe KM, Thiberge SY, Bisher ME, Burdine RD (2010). Imaging cilia in zebrafish. Methods Cell Biol 97, 415–435.

Jia Y, Xue L, Li J, Liu H (2010). Isolation and proteomic analysis of the halotolerant alga *Dunaliella salina* flagella using shotgun strategy. Mol Biol Rep 37, 711–716.

Katsanis N, Eichers ER, Ansley SJ, Lewis RA, Kayserili H, Hoskins BE, Scambler PJ, Beales PL, Lupski JR (2002). BBS4 is a minor contributor to Bardet-Biedl syndrome and may also participate in triallelic inheritance. Am J Hum Genet 71, 22–29.

Keller LC, Romijn EP, Zamora I, Yates JR, III, Marshall WF (2005). Proteomic analysis of isolated *Chlamydomonas* centrioles reveals orthologs of ciliary-disease genes. Curr Biol 15, 1090–1098.

Kramer-Zucker AG, Olale F, Haycraft CJ, Yoder BK, Schier AF, Drummond IA (2005). Cilia-driven fluid flow in the zebrafish pronephros, brain and Kupffer's vesicle is required for normal organogenesis. Development 132, 1907–1921.

Lehman JM, Michaud EJ, Schoeb TR, Aydin-Son Y, Miller M, Yoder BK (2008). The Oak Ridge Polycystic Kidney mouse: modeling ciliopathies of mice and men. Dev Dyn 237, 1960–1971.

Liu Q, Tan G, Levenkova N, Li T, Pugh EN, Jr., Rux JJ, Speicher DW, Pierce EA (2007). The proteome of the mouse photoreceptor sensory cilium complex. Mol Cell Proteomics 6, 1299–1317.

Louie CM *et al.* (2010). AHI1 is required for photoreceptor outer segment development and is a modifier for retinal degeneration in nephronophthisis. Nat Genet 42, 175–180.

Malicki J, Avanesov A, Li J, Yuan S, Sun Z (2011). Analysis of cilia structure and function in zebrafish. Methods Cell Biol 101, 39–74.

Matsuda T, Cepko CL (2004). Electroporation and RNA interference in the rodent retina in vivo and in vitro. Proc Natl Acad Sci USA 101, 16–22.

Matsuda T, Cepko CL (2007). Controlled expression of transgenes introduced by in vivo electroporation. Proc Natl Acad Sci USA 104, 1027–1032.

Mayer U, Kuller A, Daiber PC, Neudorf I, Warnken U, Schnolzer M, Frings S, Mohrlen F (2009). The proteome of rat olfactory sensory cilia. Proteomics 9, 322–334.

May-Simera HL, Kai M, Hernandez V, Osborn DP, Tada M, Beales PL (2010). Bbs8, together with the planar cell polarity protein Vangl2, is required to establish left-right asymmetry in zebrafish. Dev Biol 345, 215–225.

Muller J *et al.* (2010). Identification of 28 novel mutations in the Bardet-Biedl syndrome genes: the burden of private mutations in an extensively heterogeneous disease. Hum Genet 127, 583–593.

Ostrowski LE, Blackburn K, Radde KM, Moyer MB, Schlatzer DM, Moseley A, Boucher RC (2002). A proteomic analysis of human cilia: identification of novel components. Mol Cell Proteomics 1, 451–465.

Pan J, Wang Q, Snell WJ (2005). Cilium-generated signaling and cilia-related disorders. Lab Invest 85, 452–463.

Pathak N, Austin CA, Drummond IA (2011). Tubulin tyrosine ligase-like genes *ttll3* and *ttll6* maintain zebrafish cilia structure and motility. J Biol Chem 286, 11685–11695.

Pathak N, Obara T, Mangos S, Liu Y, Drummond IA (2007). The zebrafish *fleer* gene encodes an essential regulator of cilia tubulin polyglutamylation. Mol Biol Cell 18, 4353–4364.
Pazour GJ, Agrin N, Leszyk J, Witman GB (2005). Proteomic analysis of a eukaryotic cilium. J Cell Biol 170, 103–113.
Pazour GJ, Witman GB (2003). The vertebrate primary cilium is a sensory organelle. Curr Opin Cell Biol 15, 105–110.
Pierce EA (2001). Pathways to photoreceptor cell death in inherited retinal degenerations. Bioessays 23, 605–618.
Pierce EA, Quinn T, Meehan T, McGee TL, Berson EL, Dryja TP (1999). Mutations in a gene encoding a new oxygen-regulated photoreceptor protein cause dominant retinitis pigmentosa. Nat Genet 22, 248–254.
Riazuddin SA *et al*. (2010). A splice-site mutation in a retina-specific exon of BBS8 causes nonsyndromic retinitis pigmentosa. Am J Hum Genet 86, 805–812.
Satir P, Christensen ST (2007). Overview of structure and function of mammalian cilia. Annu Rev Physiol 69, 377–400.
Simons M, Mlodzik M (2008). Planar cell polarity signaling: from fly development to human disease. Annu Rev Genet 42, 517–540.
Singla V, Reiter JF (2006). The primary cilium as the cell's antenna: signaling at a sensory organelle. Science 313, 629–633.
Slough J, Cooney L, Brueckner M (2008). Monocilia in the embryonic mouse heart suggest a direct role for cilia in cardiac morphogenesis. Dev Dyn 237, 2304–2314.
Starich TA, Herman RK, Kari CK, Yeh WH, Schackwitz WS, Schuyler MW, Collet J, Thomas JH, Riddle DL (1995). Mutations affecting the chemosensory neurons of *Caenorhabditis elegans*. Genetics 139, 171–188.
Strauss O (2005). The retinal pigment epithelium in visual function. Physiol Rev 85, 845–881.
Vervoort R, Lennon A, Bird AC, Tulloch B, Axton R, Miano MG, Meindl A, Meitinger T, Ciccodicola A, Wright AF (2000). Mutational hot spot within a new RPGR exon in X-linked retinitis pigmentosa. Nat Genet 25, 462–466.
Westerfield M (2007). The Zebrafish Book, A Guide for the Laboratory Use of Zebrafish (Danio rerio), 5th ed., Eugene: University of Oregon Press.
Yang J, Gao J, Adamian M, Wen XH, Pawlyk B, Zhang L, Sanderson MJ, Zuo J, Makino CL, Li T (2005). The ciliary rootlet maintains long-term stability of sensory cilia. Mol Cell Biol 25, 4129–4137.
Zhang Q, Ray K, Acland GM, Czarnecki JM, Aguirre GD (2000). Molecular cloning, characterization and expression of a novel retinal clusterin-like protein cDNA. Gene 243, 151–160.